International Journal of Nanomedicine

Dovepress
open access to scientific and medical research

Open Access Full Text Article

ORIGINAL RESEARCH

Supersaturated Drug Delivery System of Oxyberberine Based on Cyclodextrin Nanoaggregates: Preparation, Characterization, and in vivo Application

Ziwei Huang[1], Shanli Zhang[1], Zehui Qin[1], Gaoxiang Ai[1], Minhua Li[1], Shiting Gong[1], Yuhong Liu[1], Huifang Zeng[2], Jiannan Chen[1], Ziren Su[1], Zhengquan Lai[3]

[1]School of Pharmaceutical Sciences, Guangzhou University of Chinese Medicine, Guangzhou, Guangdong, People's Republic of China; [2]The First Affiliated Hospital of Chinese Medicine, Guangzhou University of Chinese Medicine, Guangzhou, Guangdong, People's Republic of China; [3]Department of Pharmacy, Shenzhen University General Hospital/Shenzhen University Clinical Medical Academy, Shenzhen University, Shenzhen, Guangdong, People's Republic of China

Correspondence: Zhengquan Lai, Department of Pharmacy, Shenzhen University General Hospital/Shenzhen University Clinical Medical Academy, Shenzhen University, Shenzhen, Guangdong, People's Republic of China, Email cruise0303@163.com; Ziren Su, School of pharmaceutical sciences, Guangzhou University of Chinese Medicine, Guangzhou, Guangdong, People's Republic of China, Email suziren@gzucm.edu.cn

Propose: Oxyberberine (OBB), one of the main metabolites of berberine derived from intestinal and erythrocyte metabolism, exhibits appreciable anti-hyperuricemic activity. However, the low water solubility and poor plasma concentration–effect relationship of OBB hamper its development and utilization. Therefore, an OBB-hydroxypropyl-β-cyclodextrin (HP-β-CD) supersaturated drug delivery system (SDDS) was prepared and characterized in this work.

Methods: OBB-HP-β-CD SDDS was prepared using the ultrasonic-solvent evaporation method and characterized. Additionally, the in vitro and in vivo release experiments were conducted to assess the release kinetics of OBB-HP-β-CD SDDS. Subsequently, the therapeutic efficacy of OBB-HP-β-CD SDDS on hyperuricemia (HUA) was investigated by means of histopathological examination and evaluation of relevant biomarkers.

Results: The results of FT-IR, DSC, PXRD, NMR and molecular modeling showed that the crystallized form of OBB was transformed into an amorphous OBB-HP-β-CD complex. Dynamic light scattering indicated that this system was relatively stable and maintained by formation of nanoaggregates with an average diameter of 23 nm. The dissolution rate of OBB-HP-β-CD SDDS was about 5 times higher than that of OBB raw material. Furthermore, the $AUC_{0\text{-}t}$ of OBB-HP-β-CD SDDS (10.882 μg/mL*h) was significantly higher than that of the raw OBB counterpart (0.701 μg/mL*h). The oral relative bioavailability of OBB-HP-β-CD SDDS was also enhanced by 16 times compared to that of the raw material. Finally, in vivo pharmacodynamic assay showed the anti-hyperuricemic potency of OBB-HP-β-CD SDDS was approximately 5–10 times higher than that of OBB raw material.

Conclusion: Based on our findings above, OBB-HP-β-CD SDDS proved to be an excellent drug delivery system for increasing the solubility, dissolution, bioavailability, and anti-hyperuricemic potency of OBB.

Keywords: oxyberberine, cyclodextrin, supersaturated drug delivery systems, pharmacokinetics, hyperuricemia

Introduction

Berberine (BBR), the main active ingredient of herbal medicine Coptidis Rhizoma and Cortex Phellodendron chinense, is extensively utilized in China for the treatment of gastrointestinal disorders. Numerous studies have shown that BBR possesses a wide spectrum of pharmacological activities,[1–5] including anti-hyperuricemic and nephroprotective effects.[6] Our previous study has indicated that BBR may act as a prodrug to be metabolized into oxyberberine (OBB) in vivo to exert its pharmacological effects by intestine flora[7] and red blood cells.[8] OBB has superior bioactive activities to BBR in various diseases, including nonalcoholic fatty liver disease,[9] inflammatory diseases,[10] diabetes,[11,12] tumor,[13,14] and acute

Received: 20 February 2024
Accepted: 22 May 2024
Published: 6 June 2024

Graphical Abstract

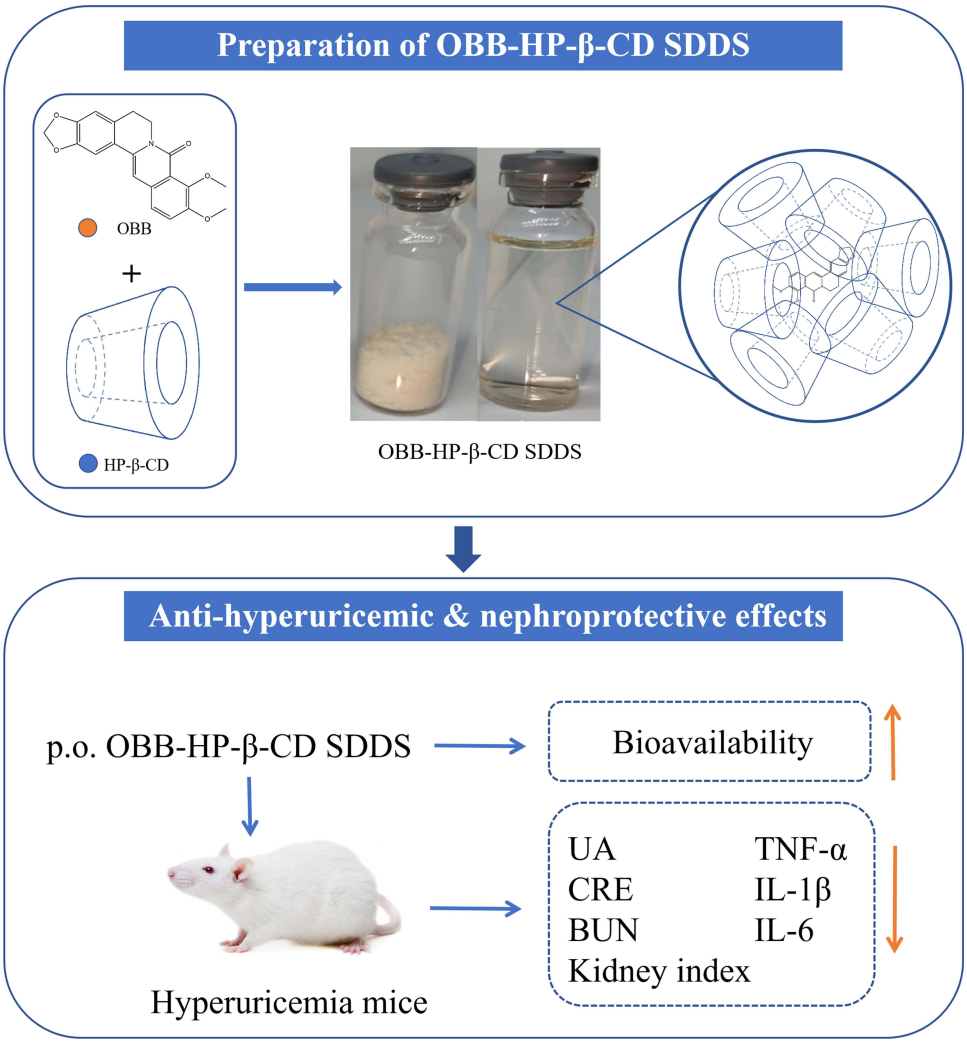

liver injury.[15,16] In particular, OBB has been found to exhibit excellent anti-hyperuricemic activity comparable to the first-line agent febuxostat in our previous study,[17,18] indicating that OBB may be a promising anti-hyperuricemic candidate. However, there is a huge gap between the physicochemical property of OBB and BBR. Due to its transformation from a quaternary ammonium structure into a more active lactam ring with decreased polarity, OBB shows lower water solubility than BBR, and most of current formulations suitable for BBR have not performed well with OBB in our preliminary experiments, which hampers its potential clinical application. Therefore, the present study aims to design an appropriate drug delivery system to improve the water solubility and bioavailability of OBB.

Cyclodextrins (CDs) are a class of naturally occurring cyclic oligosaccharides, which are traditionally used to enhance the solubility of hydrophobic drugs in pharmaceutical fields. CDs consist of a hydrophobic cavity and a hydrophilic outer surface. This cage-like structure allows them to host hydrophobic solutes, and therefore increases the water solubility.[19,20] CDs can also be used to mask irritating odors and improve the stability of guest molecules.[21,22] However, ascribed to their low aqueous solubility and nephrotoxicity, natural CDs have limited application in pharmaceuticals.[23] Hydroxypropyl-β-cyclodextrin (HP-β-CD) is one of the most commonly used derivatives of CDs. Its water solubility is significantly higher than that of natural CDs since the intramolecular hydrogen bonds of natural

CDs have been disrupted by hydroxypropyl substitution. Furthermore, according to the available research, HP-β-CD has good biocompatibility and little toxicity to humans.[24] Therefore, as an alternative to natural CDs, HP-β-CD is widely used to improve the dissolution of drugs with poor solubility in aqueous media.

In general, the limited aqueous solubility of potential drug candidates significantly hampers the drug development process. Although increasing the solubility of a compound can improve its bioavailability, researchers have found that this does not always lead to the expected increase in bioavailability.[25] This is one of the reasons why simply enhancing the apparent solubility of a drug often fails to achieve the desired bioavailability. Meanwhile, it has been suggested that supersaturation and thermodynamic activity are positively intercorrelated, and the thermodynamic activity of drugs in solution has been identified as a critical factor in drug absorption.[26] In this context, supersaturating drug delivery systems (SDDS) may offer a promising approach. These systems include amorphous phases or high-energy forms of a drug within dosage forms.[23] In the gastrointestinal tract, SDDS induce and maintain a supersaturated drug concentration, promoting the absorption of hydrophobic drugs.[27,28] However, given the inherently metastable nature of supersaturated drug solutions, their physical stabilization is essential to promote the drug absorption. This stabilization is typically achieved by incorporating excipients that inhibit crystal formation and nucleation, such as hydroxypropyl methylcellulose (HPMC) and polyvinylpyrrolidone (PVP),[29,30] while the use of other materials to maintain supersaturated drug solutions is insufficient.[27]

Current research has highlighted the potential of CDs in the development of SDDS.[31,32] In these studies, the main role of CDs was to increase the solubility of drugs, while maintaining the supersaturation of drugs was also achieved through the addition of precipitation inhibitors by different formulation techniques. However, beyond enhancing drug solubility, CDs can also maintain supersaturated solutions of drugs as precipitation inhibitors,[33–35] which may be related to the self-assembly of cyclodextrin nanoaggregates.[36] Therefore, we hypothesized that the dual properties of CDs would facilitate the stable formulation of OBB-SDDS system with increased bioavailability. Based on the promising application of HP-β-CD for drug supersaturation, our work aimed to develop OBB-SDDS based on CDs to improve the solubility and bioavailability of OBB.

In this work, OBB-HP-β-CD SDDS was characterized using differential scanning calorimetry (DSC), powder X-ray diffraction (PXRD), and Fourier transform infrared spectroscopy (FT-IR). Proton nuclear magnetic resonance (^{1}H NMR), ^{1}H-^{1}H nuclear Overhauser effect spectroscopy (^{1}H-^{1}H NOESY), and molecular modeling were used to probe the possible binding manners between OBB and HP-β-CD. The solubility, supersaturation, and dissolution properties of the system were also investigated. Furthermore, the oral bioavailability of OBB-HP-β-CD SDDS was assessed in rats. Finally, its anti-hyperuricemia activity was also evaluated. This study made pioneering endeavor to perform the pharmaceutical investigation on the metabolites of BBR, and represented the first attempt to elucidate the effect of cyclodextrins on the solubility and bioavailability of BBR metabolites from the perspective of cyclodextrin nanoaggregates-based supersaturated drug delivery system.

Materials and Methods

Chemicals and Reagents

Oxyberberine (OBB, purity > 98%) was synthesized and identified according to our previous work.[7] HP-β-CD was purchased from Xi'an DELI Biochemical Industry Co., Ltd (Xi'an, China). Methanol and acetonitrile (chromatographic grade) were purchased from Guangzhou Lubex Biological Technology Co., Ltd. (Guangzhou, China). Piperine (purity ≥ 98%) serving as the internal standard (I.S.) was purchased from National Institute for the Control of Pharmaceutical and Biological Products (Beijing, China). Potassium oxalate (PO), hypoxanthine (HX), and febuxostat (FEB) (all purity ≥ 98%) were obtained from Yuanye Biotechnology Co., Ltd. (Shanghai, China). Uric acid (UA), blood urea nitrogen (BUN), and creatinine (CRE) assay kits were procured from Jiancheng Biotechnology Co., Ltd. (Nanjing, China).

HPLC Analysis

The concentration of OBB was analyzed using the high-performance liquid chromatography (HPLC) method as previously developed by our laboratory with some modifications.[8] In this study, HPLC analysis was performed using

a Shim LC-20AD liquid chromatography system (Shimadzu, Japan). A Phenomenex Luna C18 100A column (250 mm × 4.6 mm, 5 μm) was used for chromatographic separation. The mobile phase consisted of methanol-water (70: 30, v/v) and 0.1% formic acid in water, and isocratic elution was performed at a flow rate of 1.0 mL/min at 30 °C.

Preparation and Optimization of OBB-HP-β-CD SDDS

The solubility of OBB and appropriate excipients were screened for the preparation of OBB-SDDS by solubility test. Briefly, excessive OBB was added to different dissolution media in conical flasks. All solid excipients were prepared as aqueous solutions (25 mg/mL). After that, all samples were shaken for 24 h for equilibrium solubility by using electric shaker at a rate of 90 rpm at 25°C. The samples were centrifuged (20 min, 9000 ×g) and the supernatants were obtained, filtered through a 0.22 μm microporous Millipore membrane, and diluted to a suitable concentration for HPLC analysis.

OBB-HP-β-CD SDDS was prepared by sonication and solvent evaporation, and the factors (ratio of OBB and HP-β-CD, temperature, and time) affecting the inclusion efficiency were analyzed by univariate analysis. Briefly, OBB and HP-β-CD (molar ratio 1:10) were dissolved in 95% ethanol by sonication (2 h, 40°C). When the solution was completely clear, rotary evaporation was performed to remove the solvent (65°C, 90 rpm), and the solid product was ground into powder by a mortar. Considering that the water solubility of OBB was close to zero, the insoluble part of the OBB-SDDS system in water was deemed as the free form of OBB, while the part dissolved in water was considered as bound with HP-β-CD. The inclusion efficiency (IE) prepared at different conditions was analyzed by HPLC following a previous report with some modifications.[37] First, two of equal mass samples of OBB-HP-β-CD were precisely weighed on an analytical balance (20.00 mg). The samples were then fully dissolved in a fixed volume (5.00 mL) of either water or ethanol. After centrifugation (rotating speed 10,000 ×g, 10 min), the supernatant was filtered with a microporous membrane (0.22 μm pore size), and the supernatant was taken for the determination of OBB concentration, yielding concentrations *C(ethanol)* and *C(water)*. The formula of encapsulation efficiency (IE) was as follows.

Inclusion Efficiency (IE) = C(water)/ C(ethanol)

where *C* was the concentration of OBB in water or ethanol.

To obtain controls for subsequent experiments, the physical mixture was prepared. Briefly, both OBB and HP-β-CD raw materials were placed into a mortar and gently ground into homogeneous powder to obtain the physical mixture (molar ratio of 1:10).

Phase Solubility Assay

A phase solubility study was performed using the previously described method.[38] Excessive OBB (500 mg) was added to a series of HP-β-CD (0–32 mM) aqueous solutions (50 mL). The suspensions were mixed intensively with constant stirring at 25 °C for 24 h to reach the equilibrium concentration. After that, a 0.22 μm Millipore filter was used to remove the undissolved OBB from the suspensions. The filtrate was diluted appropriately using methanol and subjected to HPLC analysis to determine the phase-solubility profiles of OBB with respect to the HP-β-CD concentrations. The stability constant (K_c), complexation efficiency (*CE*) and molar ratio (HP-β-CD: OBB) were calculated according to the following equations:

$$K_c = slope/\left[intercept^{*}(1 - slope)\right]$$
$$CE = slope/(1 - slope)$$
$$Molar\ ratio\ in\ solution\ (HP-\beta-CD : OBB) = 1 + 1/CE$$

Characterization of OBB-HP-β-CD SDDS

Fourier Transform Infrared Spectroscopy (FT-IR)

All samples were characterized by FT-IR using a Bruker Tensor 27 FT-IR spectrometer (Bruker, Germany) with a scan range of 4000–600 cm^{-1} and a resolution of 4 cm^{-1}. The background spectrum was subtracted to correct the air background spectrum. Five mg of samples with KBr was grinded on an agate mortar and compressed for 2 min at 10,000 pounds per square inch, and KBr pellets with samples were therefore prepared for analysis.

Powder X-Ray Diffractometry (PXRD)

PXRD was conducted using Rigaku D/max2500 powder X-ray diffractometer (Rigaku, Japan) equipped with a copper anode (Cu K radiation, K = 0.15405 nm, 40 kV, and 150 mA). The PXRD analysis was performed with a scanning rate of 2°/min, and the 2θ range was set to 5–90°.

Differential Scanning Calorimetry (DSC)

DSC-60 differential scanning calorimeter (Shimadzu Corporation, Japan) was used to measure the thermograms of different samples. A 40-μL aluminum crucible pan was employed to load accurately weighed samples (10 ± 0.3 mg). As a control group, a sealed empty aluminum pan was used to weigh samples. After the crucible pans were crimped, all samples were heated to 30–230°C at a rate of 10°C/min under a nitrogen atmosphere for DSC analysis.

^{1}H NMR Spectroscopy

A Bruker AC 400 MHz FT NMR spectrometer (Rheinstetten, Germany) was used to record ^{1}H NMR and ^{1}H-^{1}H NOESY spectra (673 K, 300 MHz). Both ^{1}H NMR and ^{1}H-^{1}H NOESY were performed on samples in MeOD at room temperature.

Molecular Modeling

Molecular docking is a computational technique utilized to predict the preferred orientation of two molecules and the potential to form a stable complex. A molecular modeling investigation of OBB with HP-β-CD was conducted by using AutoDockTools 1.5.6 (http://mgltools.scripps.edu/). First, the software was used to prepare all the input files. In the molecular docking process, the grid box (grid) length was set at 40 Å in each direction of the XYZ axis. The Lamarckian algorithm was used to identify the most combination of ligand molecular model. The exhaustiveness was set at 16, the maximum number of the conformational output was set at 10, and the maximum energy range was set at 3 kcal/mol. The figure was generated by PyMOL Molecular Graphics System v2.5 (Schrödinger, USA).

Self-Aggregation and Supersaturation Assays

Particle size measurement: the supersaturated solution of OBB-HP-β-CD SDDS (1 mg/mL) was prepared, and the particle size, particle size distribution (PSD) and polydispersity index (PDI) were measured just after preparation and after one hour of standing by dynamic light scattering (DLS) using a Zetasizer Nano ZS (Malvern Instruments, UK) at 25 °C.

Supersaturation stability of OBB-HP-β-CD SDDS: excessive OBB-HP-β-CD SDDS was added to artificial gastric juice or intestinal juice to prepare supersaturation. The concentrations of OBB in the supersaturation solution were equivalent to 1, 2, and 4 mg/mL, respectively. After full dissolution, samples were collected at specific time points of 5, 10, 20, 30, 45, 60, 90, 120, and 180 min. The collected samples were then subjected to filtration through a 0.22-μm membrane and subsequently analyzed by HPLC.

Dissolution Study

The in vitro dissolution study was performed using a Chinese Pharmacopoeia (2015 version) type III dissolution apparatus.[39,40] The dissolution media were 500 mL of artificial gastric or intestinal juice (37 ± 0.5 °C, 100 r/min). All samples (equivalent amount of 20 mg OBB) were encapsulated in hard gelatin capsules and submerged into dissolution media. At predetermined time intervals (5, 10, 20, 30, 45, 60, 90, and 120 min), 1.0 mL sample solutions were withdrawn and subjected to HPLC analysis after filtration through a 0.22-μm membrane. Pre-heated fresh media of equivalent volume were added each time when the media were withdrawn to maintain a constant volume. HPLC was used to determine the concentration of OBB, and the cumulative drug dissolution rate was calculated at each time point.

Pharmacokinetic Study

Eighteen male Sprague Dawley rats (male, 200–240 g) were obtained from Guangdong Medical Laboratory Animal Center (Guangzhou, China). Rats were housed in two per cage in a dark/light cycle of 12 h: 12 h with controlled

temperature and humidity. All animals were housed in laboratory conditions and fasted overnight before drug administration, with free access to water at all times. All experiments were performed in accordance with National Research Council's Guide for the Care and Use of Laboratory Animals and performed by procedures approved by the Animal Experimental Ethics Committee of Guangzhou University of Chinese Medicine (no. 20210712008).

Rats were divided into 3 groups (n = 6) and administered at a dose equal to 50 mg/kg OBB (p.o. OBB raw material, p.o. OBB-HP-β-CD SDDS and i.v. OBB-HP-β-CD SDDS). The dose selection was based on previous investigations and our pilot trial.[7,41] After administration, heparinized tubes were used to collect 250 μL of blood from the orbital vein at different predetermined intervals (0.083, 0.166, 0.25, 0.5, 1, 2, 3, 4, 5, 6, 7, 8, 12, and 24 h). The acetonitrile protein precipitation method was used to treat all the blood samples. Before measurement, 25 μL I.S. solution (20 μg/mL piperine) was added to blood samples, and centrifuged for 10 min at 2000 ×g after precipitation of samples. The residue was subjected to HPLC analysis after being redissolved in 200 μL methanol and filtered by 0.22 μm microporous membrane. The HPLC methodological details for biological sample analysis were provided in Supplementary Methods.

In vivo Anti-Hyperuricemia Studies

Seventy male KM mice (20 ± 2 g, 4 weeks) free of specific pathogens were purchased from Guangdong Medical Laboratory Animal Center (Foshan, China). For at least 7 days prior to the experiment, all mice were maintained at a constant temperature of 24 ± 1°C. All experiments were performed in accordance with the National Research Council's Guide for the Care and Use of Laboratory Animals and approved by the Ethics Committee of Guangzhou University of Chinese Medicine (No. 20210712008).

Mice were randomly assigned into the following seven groups: control (Con), model control (HUA), febuxostat (FEB), oxyberberine raw material (OBB), and three doses (1, 2, and 4 mg/kg) of OBB-HP-β-CD SDDS (OBB-SDDS) groups (n = 10). The HUA mouse model was established using hypoxanthine (HX) and potassium oxonate (PO) with some modifications.[42] Briefly, PO (300 mg/kg) was administered intraperitoneally and HX (300 mg/kg) orally once per day for 10 consecutive days to induce HUA. Physiological saline was administered to the control group at the same time points. Since the first day, all mice were administrated by gavage with saline or drug correspondingly (5 mg/kg FEB, 10 mg/kg OBB, and 1, 2, and 4 mg/kg OBB-HP-β-CD SDDS) 1 h after PO/HX challenge once daily. All drugs were administered for 7 days. The dosages of FEB and OBB were designed based on previous reports[43,44] and our pilot experiment.

Sample Collection and Calculation of Kidney Index

One hour after the final administration, all animals were anesthetized by pentobarbital sodium (50 mg/kg). Serum was separated from blood samples by centrifugation (3000 rpm, 4°C, 10 min) immediately after being collected from the abdominal aorta. The kidney was harvested, weighted, and then excised into several small sections for the following analyses. The kidney index was calculated as follows: Kidney coefficient (%) = kidney weight (g)/body weight (g)×100%. All samples were stored at −80 °C.

Biochemical Analysis

The serum UA, BUN, and CRE levels were determined using commercial kits according to the instructions of the manufacturers.

Histopathological Examination

After being removed from the mice, the kidney samples were fixed in 4% paraformaldehyde immediately. After 24 h, samples were embedded in paraffin, sliced into sections (4 μm), and stained with hematoxylin and eosin (H&E). Observations of cortexes and medullas in kidney tissue were performed under a light microscope (OLYMPUS, Japan) at 200 × magnification. Histopathology scoring was performed in a blinded manner as previously described with some modifications (Table 1).[6]

Table 1 Histopathological Scores of Kidneys in HUA Mice

Criteria		Score: Percent (%) of the Visual Field for the Respective Criteria
Glomeruli Renal tubular	Damaged glomeruli Irregular contour and dilatation Brush border loss of proximal tubular cells	0: no change 1: <15% change 2: 16–30% change
Other	Necrosis Inflammatory cell infiltration Crystalline-type deposit	3: 31–50% change 4: >50% change 5: >75% change

ELISA Assay

To prepare 10% kidney homogenate, 1:9 (w/v) saline solution was added and the mixture was homogenized on ice before centrifugation at 3000 rpm for 10 min at 4°C. The resulting supernatant was collected and subjected to enzyme-linked immunosorbent assay (ELISA) to measure the levels of IL-6, IL-1β, and TNF-α in the kidney. The ELISA assays were performed according to the manufacturer's instructions.

Statistical Analysis

The difference between groups was determined by one-way analysis of variance (ANOVA) using the SPSS version 25 software (Chicago, IL, USA). Data were expressed as mean ± standard deviation (SD). Post hoc comparisons were conducted using the turkey post hoc test when the *F* ratios were significant. *P* values less than 0.05 were considered as statistical significance.

Results and Discussion

Preparation of OBB-HP-β-CD SDDS

The molecular structures of OBB and HP-β-CD used in this study are shown in Figure 1A and B. Firstly, the solubility of OBB was investigated in this study (Figure 1C and Table 2). OBB was only slightly soluble in artificial gastric juice (about 0.32 μg/mL) and completely insoluble in intestinal juice and distilled water (cannot be detected), which might be ascribed to its weak basic isoquinoline alkaloids skeleton. These results indicated that the dissolution of OBB post oral administration was found to primarily occur in the gastric juice with a sufficiently low pH. However, upon entering the small intestine, which had a higher pH compared to the stomach, the solubility of OBB was significantly reduced. This reduction in solubility could lead to precipitation prior to absorption.

To improve the dissolution of OBB, many excipients were used for multiple attempts to prepare OBB-SDDS. The results showed that the solubility of OBB in multiple excipients was extremely low, while only HP-β-CD and sulfobutyl ether-β-cyclodextrin gave satisfactory results for improving the solubility of OBB, potentially ascribed to superior physical or chemical interaction between OBB and CDs. However, due to its excessive hygroscopicity, sulfobutyl ether-β-cyclodextrin proved challenging to prepare OBB-SDDS. Meanwhile, considering the high cost associated with cyclodextrins, HP-β-CD was ultimately selected as the preferred excipient for OBB-SDDS preparation.

Subsequently, the phase solubility technique was used to investigate the effect of HP-β-CD on the solubility of OBB. Figure 1D illustrates the phase solubility diagrams of OBB with HP-β-CD in distilled water at 37 ± 0.5°C. The aqueous solubility of OBB increased linearly with HP-β-CD concentration (r = 0.9991) ranging from 0 to 32 mM, indicative of A_L-type solubility diagram (1:1 inclusion complex).[45] The stability constants (*Ks*) of OBB were calculated. An excessively high *Ks* usually means that the strong interaction between drugs and HP-β-CD may hinder the release of the drug. While an excessively low *Ks* means drugs cannot bind with HP-β-CD. The *Ks* of OBB-HP-β-CD was 199.992 M^{-1}, which fell within the range of 100–1000 M^{-1}, indicating that this complex was appropriately stable.[46] Meanwhile, the complexation efficiency (CE) value of OBB-HP-β-CD was 0.038, which indicated that a quantity of 26.6 molecules

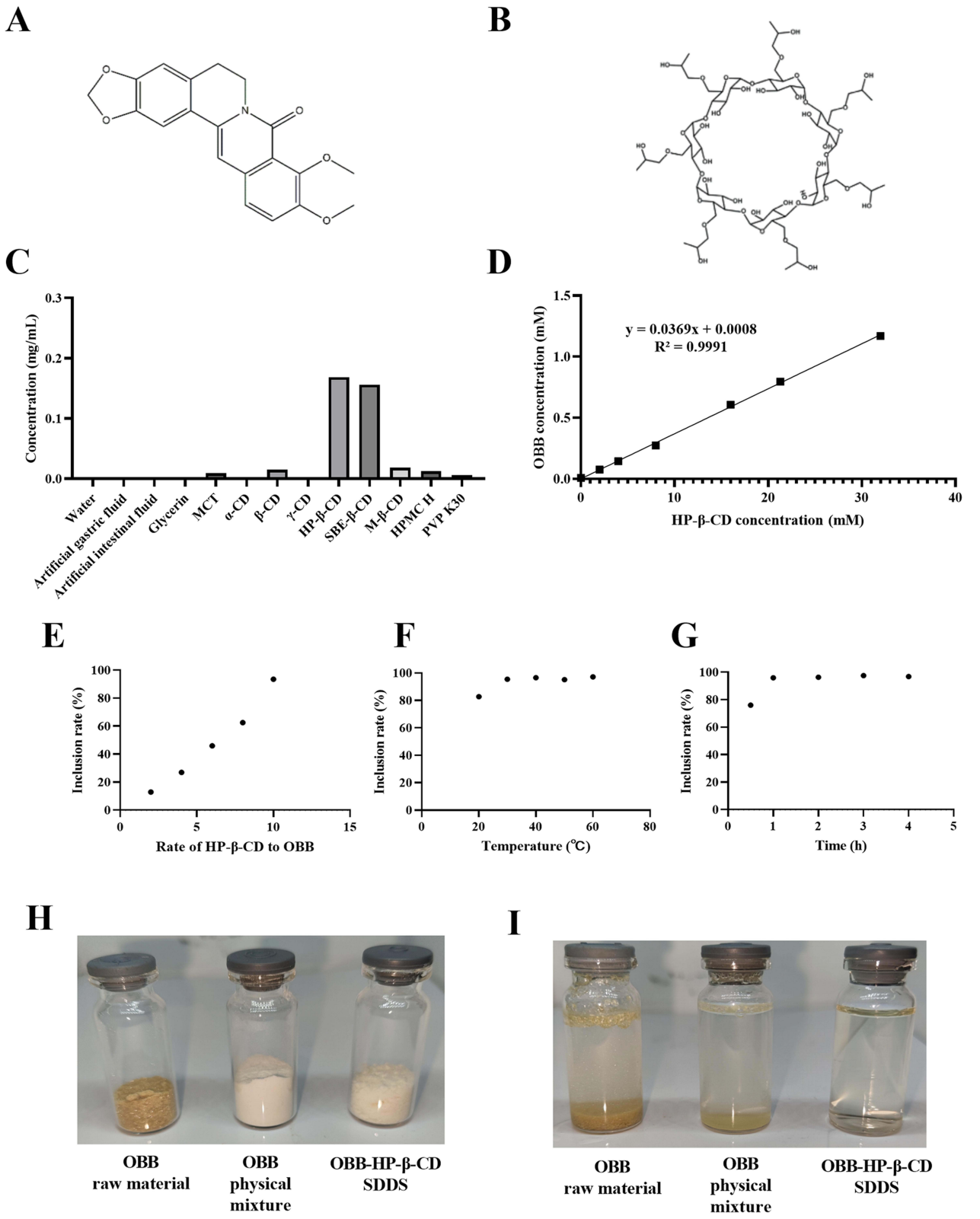

Figure 1 Preparation and optimization of OBB-HP-β-CD SDDS. The structures of OBB (**A**) and HP-β-CD (**B**). Effect of different excipients on the solubility of OBB (**C**). Phase solubility diagram for OBB-HP-β-CD system (**D**). Effect of feed ratio (**E**), temperature (**F**) and reaction time (**G**) on the inclusion efficiency. The appearances of different samples before (**H**) and after (**I**) dissolved in water.

Table 2 The Solubility of OBB Raw Material in Different Dissolution Media

Dissolution Medium	Solubility (μg/mL)
Water	< 0.05 (cannot be detected)
Artificial gastric fluid	0.32
Artificial intestinal fluid	< 0.05 (cannot be detected)

of HP-β-CD was sufficient to facilitate the dissolution of a single molecule of OBB, possibly ascribed to the formation of nanoaggregates of HP-β-CD.

To further optimize the preparation process, three factors affecting the preparation of OBB-HP-β-CD SDDS were preliminarily investigated by univariate analysis. The inclusion rate was used as the evaluating index, and the inclusion efficiency was equivalent to the ratio of soluble forms of OBB. The results are presented in Figure 1E-G. For OBB, the inclusion efficiency and degree of supersaturation were only improved with an increased amount of HP-β-CD, which could reach up to 100% approximately. However, other factors such as temperature and time, had almost no effect on the inclusion efficiency and solubility of OBB. Therefore, the inclusion efficiency of OBB-HP-β-CD SDDS used in the subsequent experiments was 100% approximately (molar ratio 1:10).

To our knowledge, OBB-HP-β-CD SDDS was prepared for the first time. As shown in Figure 1H and I), the samples of OBB raw material were khaki crystals, while OBB-HP-β-CD SDDS and the physical mixture were white or pale-yellow powder. After the addition of water and sufficient stirring, the systems of both OBB raw material and OBB-HP-β-CD physical mixture remained cloudy. In contrast, the OBB-HP-β-CD SDDS could be quickly transformed into a pale-yellow clear solution. This observation indicated that the water solubility of OBB could be significantly improved by OBB-HP-β-CD SDDS. Furthermore, the solubility of the prepared samples in water appeared to have no definite limit (at least exceeding 4 mg/mL, calculated as OBB). However, upon standing for a period, slow precipitation could be observed, which indicated that OBB supersaturation solutions were formed, and this outcome was inconsistent with traditional drug-CD inclusion complexes.[35] Therefore, the sample was considered to have formed a supersaturated system after dissolution.

Characterization of OBB-HP-β-CD SDDS

Figure 2A shows the FTIR spectra of different samples. As depicted from the spectrum of OBB, there were characteristic peaks at various absorption bands including 1643, 1618, 1595, 1493, 1379, 1276, 1222, 1084, and 1036 cm^{-1}. As a result of symmetric and asymmetric stretching modes of O//H and C//H bonds, pure HP-β-CD showed characteristic peaks at 3405 cm^{-1} and 2929 cm^{-1}, respectively. Most of the OBB characteristic peaks were masked in the superimposition of HP-β-CD, which might be due to low OBB content in OBB-HP-β-CD physical mixture. However, some characteristic peaks of OBB, such as 1643, 1493, and 1276 cm^{-1}, could still be found in OBB-HP-β-CD physical mixture, indicative of no potential interaction. However, all the characteristic peaks disappeared in the spectrogram of OBB-HP-β-CD SDDS. These FTIR results also suggested that OBB and HP-β-CD might interact mutually.

PXRD experiments can provide information on the crystallinity of all samples. Figure 2B illustrates the sharp diffraction peaks of OBB raw material, indicative of high crystallinity.[47] In contrast, HP-β-CD exhibited no characteristic peaks of crystal in its spectrum, suggestive of amorphous state. The physical mixture was characterized by the superposition of OBB and HP-β-CD, with the characteristic peak of OBB, indicating that there was no interaction in the OBB-HP-β-CD physical mixture. However, the diffractograms of OBB-HP-β-CD SDDS, which were quite similar to those of HP-β-CD, did not show any characteristic peak of OBB in its spectrum. This diffractogram implied that OBB might exist as an amorphous form in HP-β-CD SDDS, indicating that there was host-guest inclusion interaction.

It was possible that the melting, boiling, or sublimation point of OBB-HP-β-CD SDDS shifted or disappeared before decomposing if OBB molecule was embedded in the cavities of HP-β-CD. Therefore, OBB-HP-β-CD SDDS were investigated using differential scanning calorimetry (DSC). The results are shown in Figure 2C. As a typical crystalline substance, OBB showed a sharp endothermic peak at 203°C, which corresponded to its melting point. The intensity of the

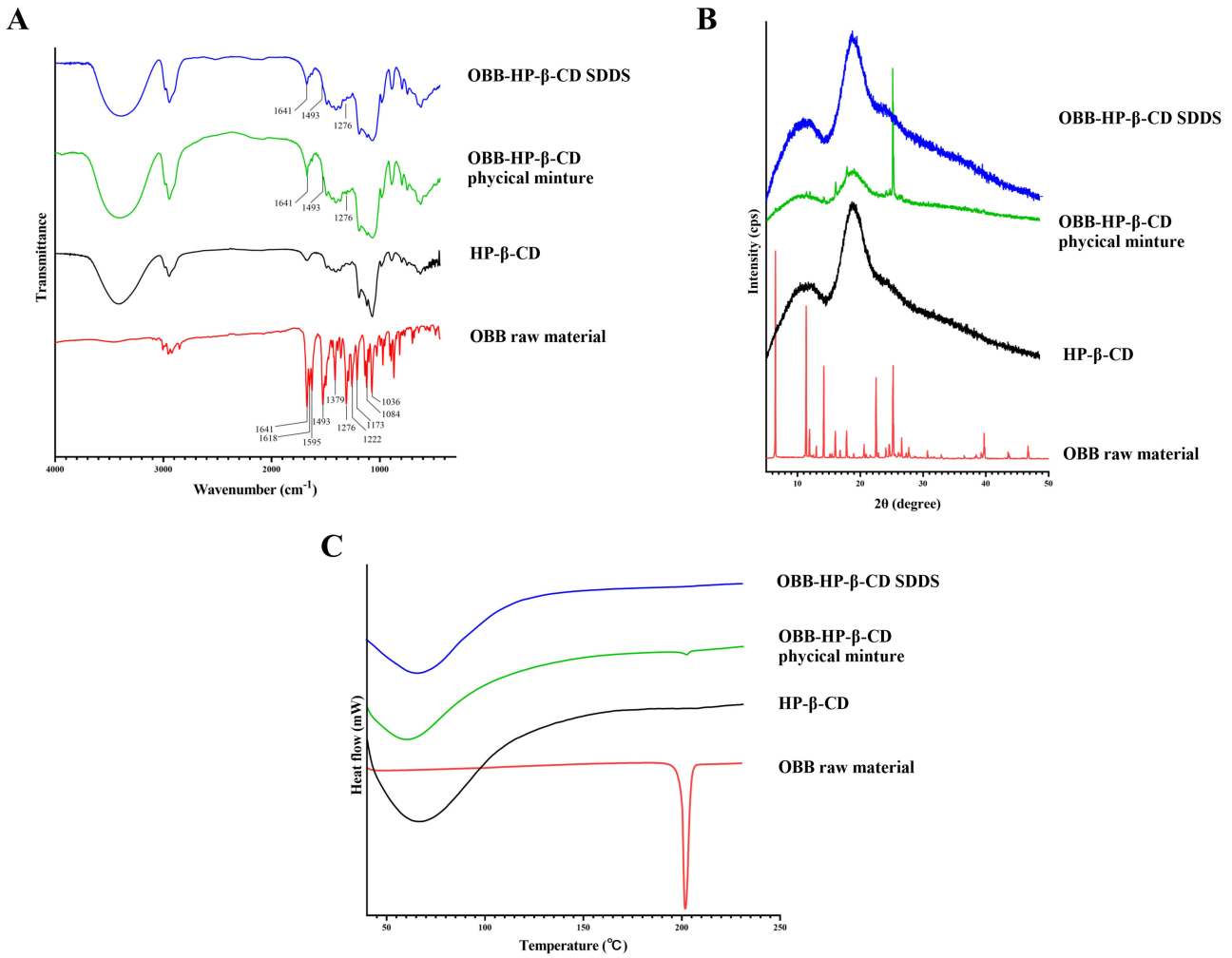

Figure 2 FT-IR (**A**), PXRD (**B**), and DSC (**C**) thermograms of OBB, HP-β-CD, OBB-HP-β-CD physical mixture, and OBB-HP-β-CD SDDS. The figures were generated by GraphPad prism 8.

endothermic peak of OBB in the OBB-HP-β-CD physical mixture partially decreased but did not disappear, while the peak intensity of OBB in OBB-HP-β-CD SDDS completely disappeared in DSC curves from the same content of OBB. These results showed that OBB could be embedded in cavities of HP-β-CD by sonication and solvent evaporation.

From these results, we could infer interaction between OBB and HP-β-CD. Nevertheless, it was crucial to obtain further structural insights by ^{1}H NMR spectroscopy.[48,49] Chemical shifts provided detailed information on the chemical environment of an atom, and the sole difference in the chemical environment of OBB protons between OBB and OBB-HP-β-CD SDDS was the steric and ring-current effects between OBB and HP-β-CD.[50] Therefore, the chemical shift changes of different hydrogen atoms of OBB suggested the possible binding site to HP-β-CD. Figure 3A shows the ^{1}H NMR spectra of HP-β-CD, OBB, and OBB-HP-β-CD SDDS.

Table 3 shows the difference in chemical shift values of OBB protons in OBB raw material and OBB-HP-β-CD SDDS, where Δδ = δ (OBB-HP-β-CD SDD–) - δ (OBB raw material). The chemical shifts of H-11, H-13, 9-OCH_3, 10-OCH_3, and O-CH_3-O of OBB were changed in HP-β-CD SDDS, and the chemical shift of protons of 9-OCH_3 and 10-OCH_3 exhibited more significant changes than other protons, indicating that the 9, 10-methoxyl might bind with HP-β-CD more tightly than other sites. Further confirmation of HP-β-CD and OBB host–guest interactions was obtained through ^{1}H-^{1}H NOESY. There were visible cross-peaks in the NOESY spectrum resulting from interaction between HP-β-CD and OBB (Figure 3B), suggesting that there was enough nearness between HP-β-CD and OBB for nuclear

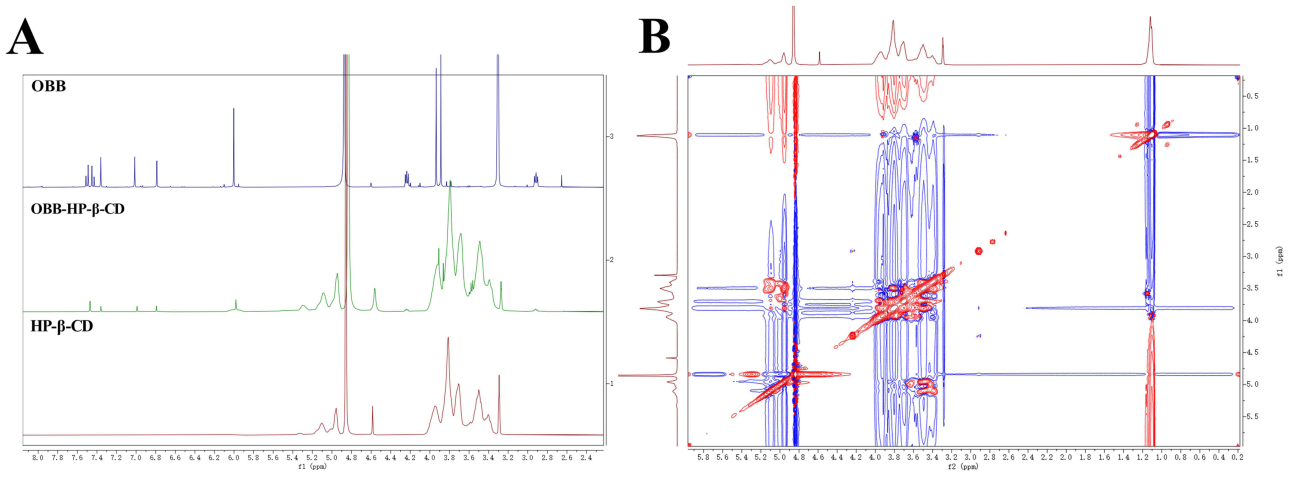

Figure 3 ^{1}H NMR diffractogram (**A**) of OBB, HP-β-1CD, OBB-HP-β-CD physical mixture, OBB-HP-β-CD SDDS and ^{1}H-^{1}H NOESY diffractogram (**B**) of OBB-HP-β-CD SDDS.

overhauser effect (NOE) correlations to occur.[51] These results indicated that OBB could interact with the protons of HP-β-CD where it was accommodated.

Furthermore, molecular modeling was employed to examine the interaction of OBB and HP-β-CD. The docked conformations of OBB bound to HP-β-CD are shown in Figure 4. The result indicated that the interaction of OBB with HP-β-CD was generated mainly by the proton of 9, 10-methoxyl of OBB, corroborating the findings from the 1H-NMR analysis. The binding affinity of OBB at HP-β-CD was −4.3 kcal/mol, indicating that the complex was not stable. This result was overall consistent with the preceding result that the supersaturated solution of OBB was not completely stable. Meanwhile, previous report has suggested that the maintenance of drug supersaturation by CDs was less related to the inclusion complex formation between CDs and drugs,[35] which also indicated that OBB-HP-β-CD SDDS was different from traditional drug-cyclodextrin inclusion complex. Despite this, OBB-HP-β-CD SDDS did display an extremely excellent solubilization effect of OBB. Consequently, further research was warranted to explore the supersaturation and druggability of OBB-HP-β-CD SDDS.

Self-Aggregation and Supersaturation Assays

In this section, we further delineated the solubilization effect of OBB-HP-β-CD SDDS. As shown in Figure 5A, when the supersaturated solution was freshly prepared, its particle size could not be detected, indicating that the entire system was a true solution of OBB-HP-β-CD complex at this time. Subsequently, the system was left to stand for an hour and the resulting particle size was analyzed by DLS analyzer. The result revealed that the average particle size of CD-aggregates in the system was 45.14 nm, and the PDI was 0.508. Interestingly, the particle size distribution exhibited two peaks at this

Table 3 The Chemical Shift of OBB Raw Material and OBB-HP-β-CD SDDS

Proton	δ (OBB Raw Material)	δ (OBB-HP-β-CD SDDS)	Δδ (ppm)
O-CH3-O	6.00	5.98	0.02
H-4	6.79	6.79	0.00
H-5	2.92	2.92	0.00
H-6	4.23	4.23	0.00
9-OCH3	3.91	3.94	0.03
10-OCH3	3.91	3.94	0.03
H-11	7.47	7.47	0.00
H-12	7.36	7.36	0.00
H-13	7.01	6.99	0.02

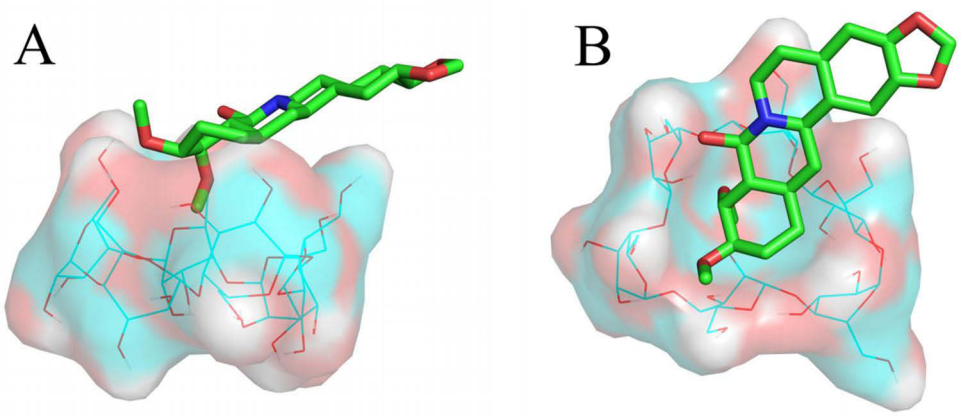

Figure 4 Surface view of the binding configuration of OBB and HP-β-CD in molecular modeling, showing the 9 or 10-methoxyl of OBB inside the cavity of HP-β-CD. (**A**) Front view. (**B**) Top view. The figures were generated by PyMOL Molecular Graphics System (version 2.5).

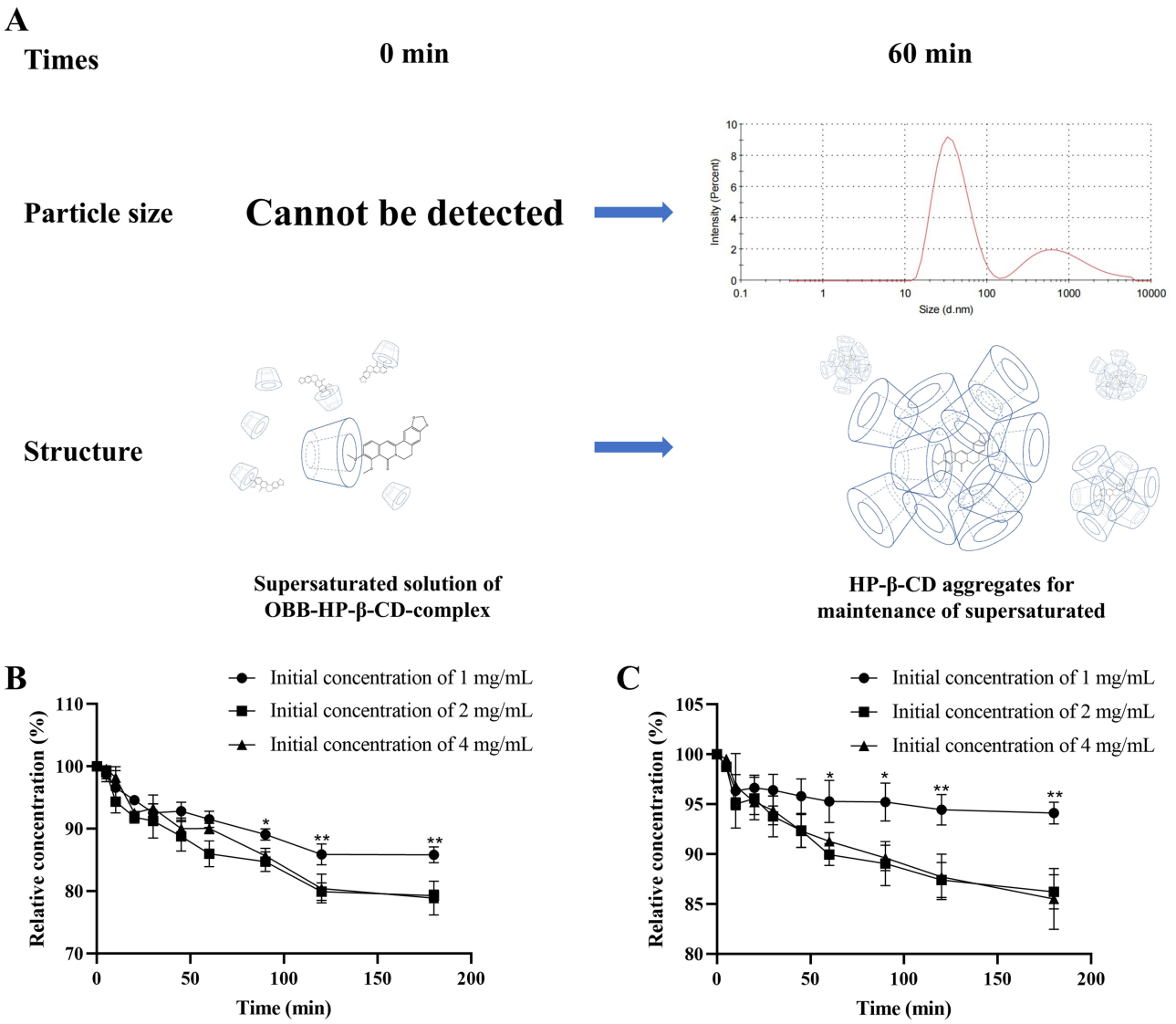

Figure 5 The formation of nanoaggregates in OBB-HP-β-CD SDDS to maintain supersaturation. The shift of particle size and its potential nanoaggregates structural diagram (**A**), and its supersaturated stability in artificial gastric (**B**) and intestinal (**C**) juice (n = 3). *p < 0.05 and **p < 0.01 vs 4 mg/mL group.

point, with the average particle sizes of 40.60 (72.5%) and 1049.00 nm (27.5%), respectively. Additionally, a small quantity of white flocculent precipitate was observed in the system rather than yellow OBB crystals. However, no significant nanoaggregates were detected at the same concentration of blank HP-β-CD solution.

The solution stability of supersaturation is shown in Figure 5B and C. In this assay, the drug concentration–time curve of OBB supersaturation solution decreased smoothly without a significant "spring effect",[52,53] indicating OBB-HP-β-CD SDDS rapidly formed OBB supersaturation system in different dissolution media. Besides, though HP-β-CD was acid-labile, there was no difference found in the drug concentration–time curve between artificial gastric fluid and intestinal fluid. One of the possible reasons was that an excessive amount of HP-β-CD maintained the stability of this system in an acidic environment to some extent.

Obviously, the excess of cyclodextrins was the most important factor in forming a supersaturated solution. In general, drug supersaturation was sustained mainly by preventing nucleation and/or inhibiting crystal growth. Hydrogen-bonding interactions served as the primary mechanism for precipitation inhibitors and also facilitated the entry of hydrophobic drugs into the hydrophobic cavity of HP-β-CD. Furthermore, preceding study has reported that HP-β-CD, ascribed to its hydroxypropyl substitution, exhibited enhanced surface activity compared to natural cyclodextrins. This attribute significantly contributed to its more effective inhibition of crystallization.[35]

More importantly, despite the conflicting studies on the formation of aggregates by HP-β-CD,[54] this study indicated that polymer particles could be detected in the supersaturated solution of OBB-HP-β-CD SDDS after 60 min of incubation. In previous studies, there was a tendency for the HP-β-CD molecules to spontaneously form aggregates by network of hydrogen bonds[55,56] when a critical concentration was exceeded, this tendency was spontaneous and exothermic. Simultaneously, drug molecule may also be a crucial factor inducing the formation of cyclodextrin nanoclusters.[57] In the earlier section of our study, OBB was observed not to fully embed within the cavity of HP-β-CD, resulting in a substantial exposure of hydrophobic structure outside the OBB-HP-β-CD complex. This exposure might lead to a tendency for mutual aggregation and crystallization among OBB-HP-β-CD molecules, inducing the formation of OBB-HP-β-CD self-aggregates. Simultaneously, this process may be accompanied by a self-aggregation phenomenon inherent to the HP-β-CD branches. while the self-aggregates formed around OBB molecules may influence the inherent self-aggregation tendency of HP-β-CD. These closely interacting molecules emerged as potential key contributors inducing the formation of nanoclusters, and this also resulted in aggregation behaviors that differed from those of pure cyclodextrins. More importantly, this process may inhibit the aggregation of OBB molecule by steric hindrance, and thus inhibit crystallization and maintain supersaturation (Figure 5A).

Additionally, during the process of solvent evaporation (eg solid dispersion technique), the CD-drug complex might become homogeneously dispersed within the excessive cyclodextrin matrix in either molecular or amorphous state. This dispersion promoted the formation of an initial supersaturated concentration of the OBB-HP-β-CD complex. These observations collectively contributed to the supersaturation of OBB in OBB-HP-β-CD SDDS, which provided novel insight into the solubilization of HP-β-CD. However, further investigation was merited to elucidate the specific mechanism by which cyclodextrin maintained the supersaturated state of OBB.

Dissolution and Pharmacokinetics

The dissolution profile of OBB-HP-β-CD SDDS and the physical mixture are shown in Figure 6. The cumulative release percentage of the physical mixture was less than 23% in artificial gastric fluids and 15% in intestinal fluids after 180 min, respectively. In contrast, the release percentage of OBB-HP-β-CD SDDS was higher than 95% within 20 min, indicating that the dissolution rate of OBB-HP-β-CD SDDS was significantly higher than that of the physical mixture in a pH-independent manner. Consequently, OBB-HP-β-CD SDDS was deemed as an effective and feasible strategy to improve the dissolution efficiency o1f OBB.

In the pharmacokinetics study, a sensitive HPLC method was established. The HPLC methodological quality assessment indicated that the method was reliable and reproducible for biological sample analysis (Supplementary Materials, Tables S1-S3, Figure S1). Though the water solubility of OBB was significantly lower than that of BBR, the oral bioavailability of OBB (1.55%, Table 4) was significantly higher than the BBR counterpart as previously reported,[58,59] which might be attributed to its higher lipophilicity and intestinal permeability.

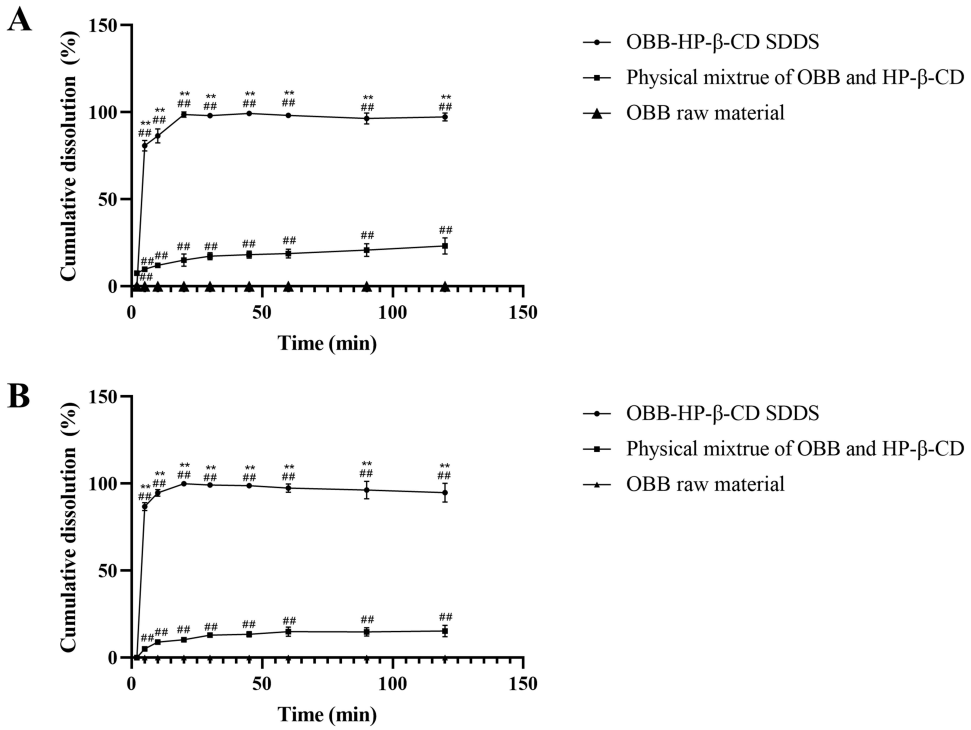

Figure 6 Dissolution profiles of OBB raw material and OBB-HP-β-CD SDDS in artificial gastric (**A**) and intestinal (**B**) juice (n = 3). ##p < 0.01 vs OBB raw material; **p < 0.01 vs physical mixture of OBB and HP-β-CD.

The concentration–time profiles and pharmacokinetic parameters of OBB and OBB-HP-β-CD SDDS in rats are shown in Figure 7 and Table 4, respectively. These results revealed that the AUC_{0-t} and C_{max} of OBB-HP-β-CD SDDS were 10.882 μg/mL*h and 2.486 μg/mL, respectively, which were 15.32 and 10.66 times higher than those of OBB raw material. The bioavailability of OBB-HP-β-CD SDDS was calculated to be 24.73%, indicative of a 15.55-fold increase compared to that of OBB raw material. Hence, OBB-HP-β-CD SDDS could significantly improve the bioavailability of OBB compared to the raw material. The observed enhancement in bioavailability could be attributed to the rapid formation of OBB supersaturation by OBB-HP-β-CD SDDS upon exposure to the gastrointestinal environment, sustaining this supersaturated state until T_{max}. However, further in-depth investigation was warranted to probe the exact mechanism.

In this process, the interaction between HP-β-CD and the lipophilic surface of biological membranes, altered the sorption-desorption equilibrium of drugs complexes, resulting in improved absorption of this bioactive compound.[54] More importantly, the supersaturation significantly enhanced the thermodynamic activity of OBB, further improving the

Table 4 Pharmacokinetic Parameters of OBB

Parameter	p.o. OBB Raw Material (50 mg/kg)	p.o. OBB-HP-β-CD SDDS (50 mg/kg)	i.v. OBB-HP-β-CD SDDS (10 mg/kg)
AUC_{0-t} (μg/mL*h)	0.701 ± 0.340	10.882 ± 2.606**	8.801 ± 1.662**
$AUC_{0-\infty}$ (μg/mL*h)	0.985 ± 0.379	11.225 ± 2.145**	9.283 ± 1.522**
$T_{1/2z}$ (h)	1.567 ± 0.511	3.118 ± 1.348	0.097 ± 0.031**
C_{max} (μg/mL)	0.233 ± 0.059	2.486 ± 0.400**	7.809 ± 0.845**
Clz/F (L/h/kg)	61.986 ± 31.406	4.689 ± 1.243**	1.103 ± 0.160**
$T0_{max}$ (h)	4.667 ± 0.471	4.167 ± 0.373	-

Notes: **p < 0.01 vs p.o. OBB raw material group.

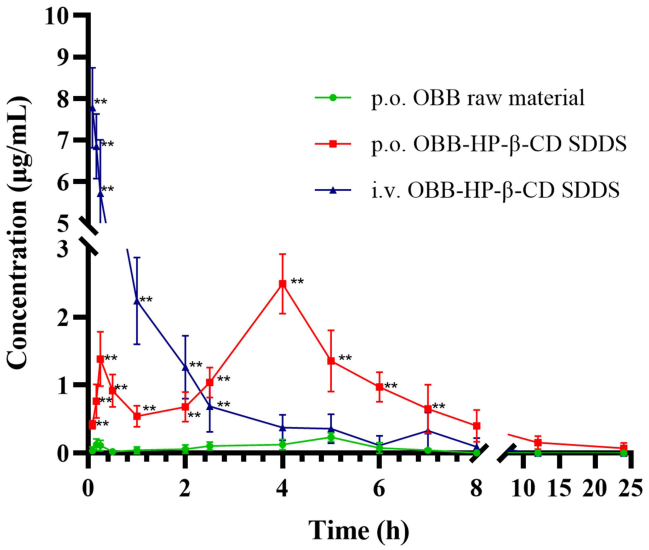

Figure 7 Plasma concentration–time curves of OBB raw material and OBB-HP-β-CD SDDS in rats (n = 6). **p < 0.01 vs p.o. OBB raw material.

driving force for targeting the biological membrane[60] and enhancing its intestinal permeability in this process. These factors together potentially contributed to the improvement of the bioavailability of OBB in OBB-HP-β-CD SDDS.

In vivo Anti-Hyperuricemia Study

In our previous study, OBB has been found to exhibit pronounced anti-hyperuricemic and nephroprotective effects.[17,18] In the present work, the HUA mouse model was employed to evaluate the potential anti-hyperuricemia of OBB-HP-β-CD SDDS.

In addition to the anticipated improvement in oral bioavailability, the developed OBB-HP-β-CD SDDS resulted in the enhancement of biological activity. As shown in Figure 8A, there was a substantial increase in the serum UA level subjected to PO and HX treatment, indicative of successful establishment of the HUA model. Compared with the HUA group, administration of FEB and OBB raw material significantly decreased the serum UA level in HUA mice. Notably, treatment with OBB-HP-β-CD SDDS resulted in a more obvious decline in UA level at lower dose compared with OBB raw material. These results indicated that OBB-HP-β-CD was remarkably effective for the alleviation of serum UA accumulation.

HUA was commonly linked to renal impairment, and the serum levels of creatinine (CRE) and blood urea nitrogen (BUN) were markers of renal function. The results depicted in Figure 8B-D indicated a marked rise in the serum levels of CRE and BUN, and a concurrent increase in the kidney index in HUA group, indicative of renal dysfunction. Histopathological examination further supported this result. As illustrated in Figure 9, kidneys in HUA mice exhibited inconspicuous boundaries, atrophied glomeruli, and proximal tubules with lost brush borders, while the renal tissues in the Con group had normal histological structure and architecture. Meanwhile, inflammation was one of the main factors in HUA-induced kidney injury. As shown in Figure 10, HUA caused significant increases in TNF-α, IL-1β, and IL-6 levels in the kidneys of mice with renal injury.

However, treatment with OBB-HP-β-CD SDDS, OBB raw material, and FEB reversed the kidney damage induced by HUA to varying degrees. The kidney index and serum level of BUN were significantly reduced after treatment with different drugs. Notably, only OBB-HP-β-CD SDDS (4 mg/kg) treatment significantly decreased the serum CRE level compared with the HUA group ($P < 0.05$). Additionally, histopathological analysis revealed that OBB-HP-β-CD SDDS, OBB raw material, and FEB all effectively ameliorated renal histopathological damage compared to the HUA group. Although some improvement in the proximal convoluted tubules could be observed, there were still severe dilation of renal tubules and disruption of the glomeruli capsules in the proximal tubules in HUA mice receiving low-dose (1 mg/kg) OBB-HP-β-CD SDDS. However, middle- (2 mg/kg) and high-dose (4 mg/kg) OBB-HP-β-CD SDDS proved effective in

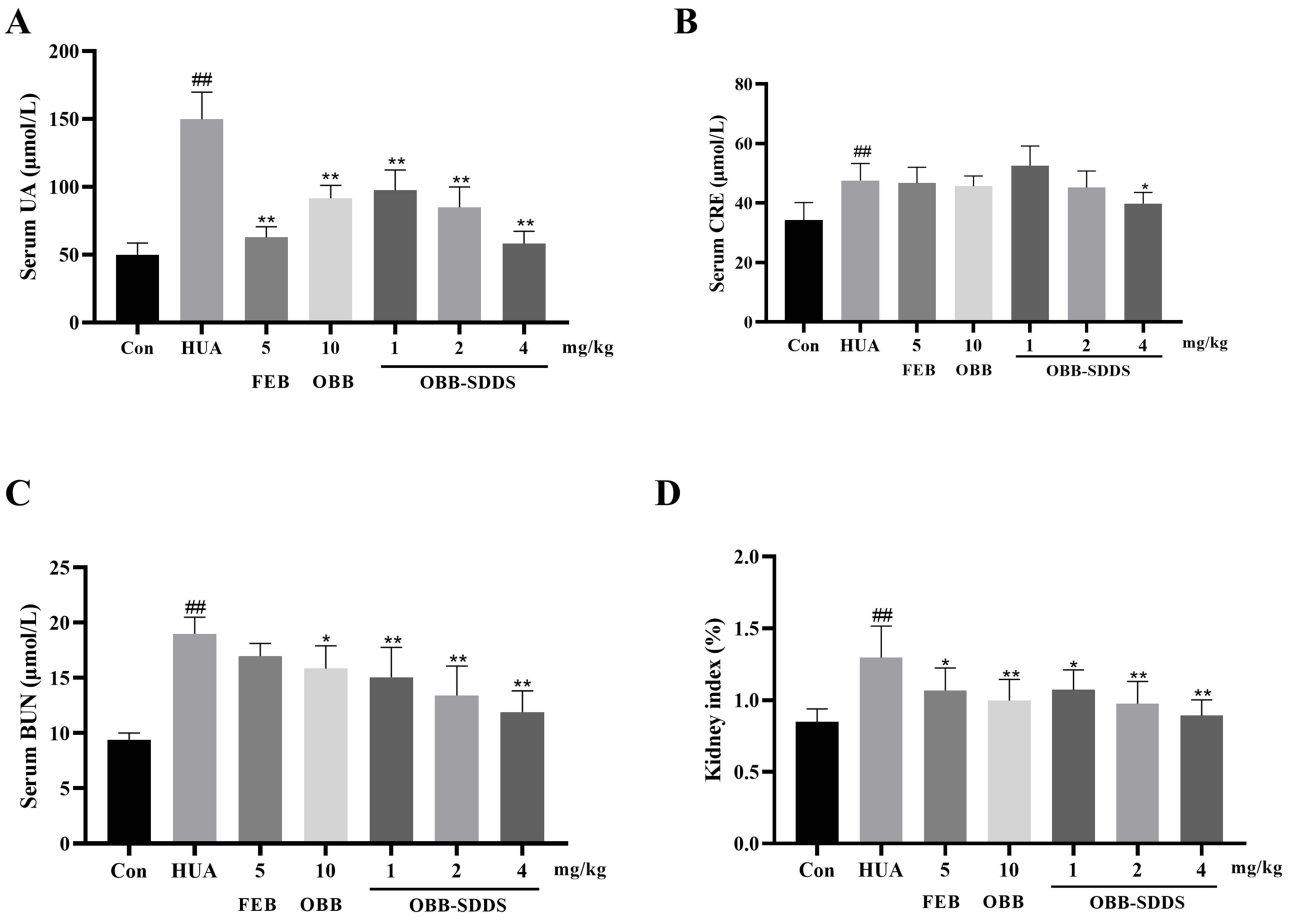

Figure 8 Effect of OBB-HP-β-CD SDDS on serum levels of UA (**A**), CRE (**B**) and BUN (**C**), and kidney index (**D**) in HUA mice. Data are shown as mean ± SD (n = 10). $^{\#\#}p < 0.01$ vs Con group. *p < 0.05 and **p < 0.01 vs HUA group.

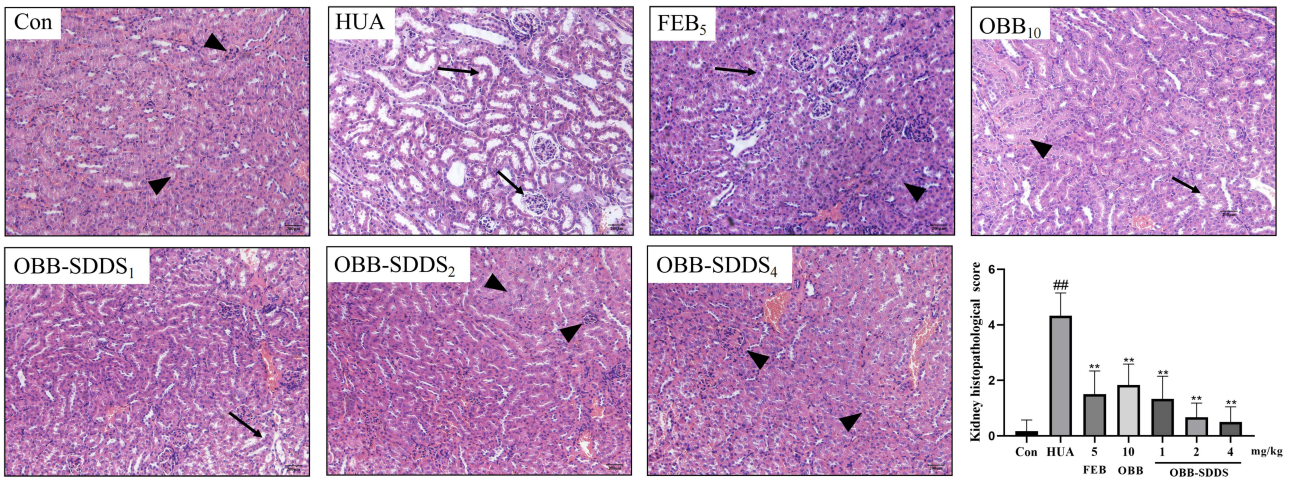

Figure 9 H&E staining (200 ×) and histopathological score of kidney sections in HUA mice (n = 3). Black arrow: atrophic glomeruli and unusual tubular structure; black arrowhead: normal renal tubular and glomeruli. $^{\#\#}p < 0.01$ vs Con group; **p < 0.01 vs HUA group.

attenuating the glomeruli and tubule damages. Meanwhile, treatment with OBB-HP-β-CD SDDS significantly and dose-dependently reversed the increased levels of inflammatory factors TNF-α, IL-1β, and IL-6 (Figure 10).

In summary, our results suggested that OBB-HP-β-CD SDDS showed excellent anti-hyperuricemic and nephroprotective effects. It was noteworthy that the efficacy of 1–2 mg/kg OBB-HP-β-CD SDDS was approximately equal to

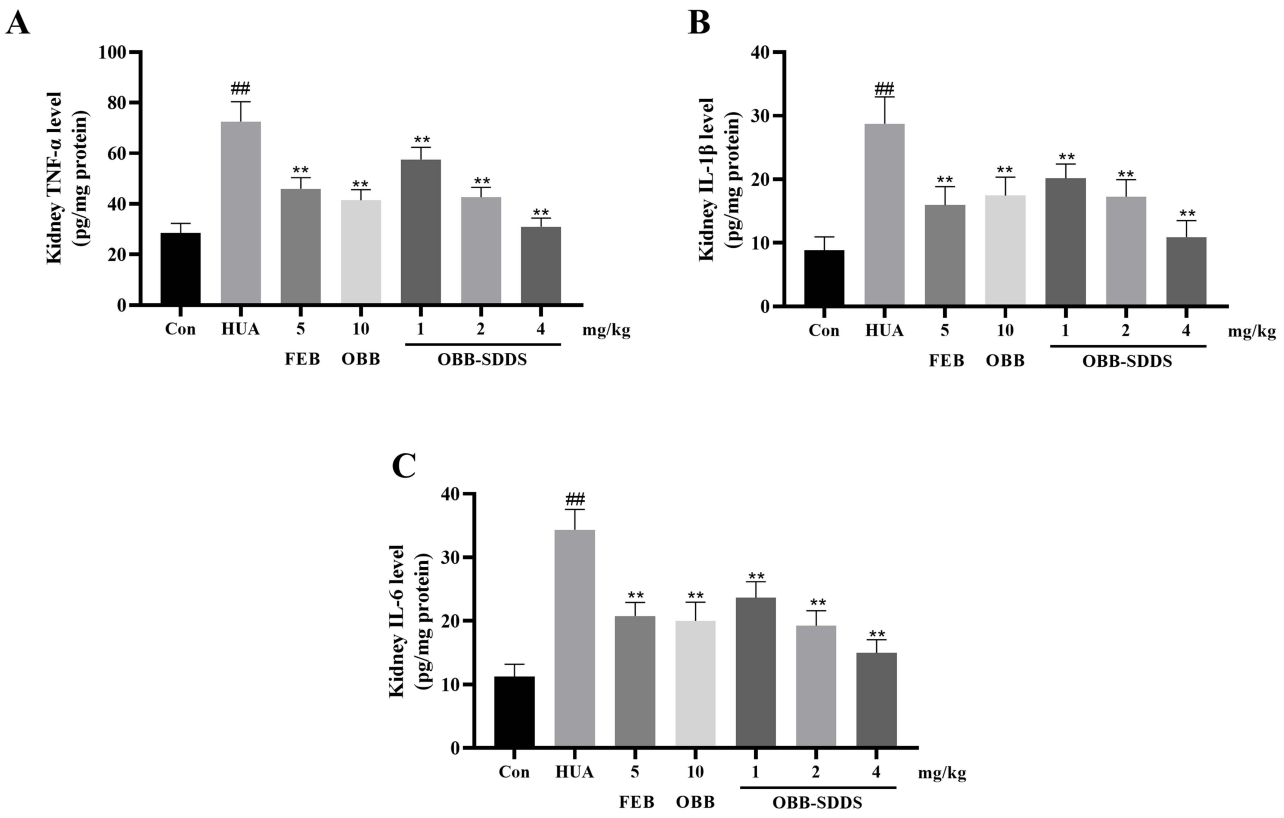

Figure 10 Effect of OBB-HP-β-CD SDDS on inflammatory cytokines in HUA mice (n = 10). (**A**) TNF-α, (**B**) IL-1β, and (**C**) IL-6. ##p < 0.01 vs Con group; **p < 0.01 vs HUA group.

10 mg/kg OBB raw material, indicating that the bioactivity of OBB was significantly accentuated by OBB-HP-β-CD SDDS (approximately 5–10 times higher than OBB raw material). Therefore, OBB-HP-β-CD SDDS represented a feasible approach to improve the potency and druggability of OBB. However, although previous study have indicated that the raw OBB agent has a favorable safety profile, the comprehensive safety evaluation of OBB-HP-β-CD SDDS is desired.[18] Also, this work has not yet provided the detailed anti-hyperuricemic mechanism in vivo and in vitro in different models. Future studies for elucidating the safety and detailed molecular mechanism underlying the anti-hyperuricemic effect of OBB-HP-β-CD SDDS would likely pave an avenue for promising drug development process.

Conclusions

OBB-HP-β-CD SDDS was prepared and characterized for the first time. Compared with OBB raw material, OBB-HP-β-CD SDDS could be rapidly dissolved in various dissolution media to create a relatively stable supersaturated solution of OBB, and the supersaturation of OBB was maintained by aggregation of HP-β-CD. Furthermore, the absorption, bioavailability and potency of OBB could be enhanced by HP-β-CD-SDDS. Therefore, OBB-HP-β-CD SDDS was a feasible and effective technique for enhancing the biopharmaceutical properties of OBB. This work provided experimental support for the preparation of OBB for oral administration and revealed an enlightening paradigm, highlighting that HP-β-CD-based SDDS might be a promising strategy for improving the druggability of bioactive alkaloids with low water solubility.

Acknowledgments

This work was supported by grants from the Science and Technology Planning Project of Shenzhen City (No. JCYJ20220531103010022), the Traditional Chinese Medicine Bureau of Guangdong Province (No. 20221331), the National Natural Science Foundation of China (Nos. 82074082 & 82104472), and the Natural Science Foundation of

Guangdong Province (Nos. 2021B1515140003 & 2021A1515011490 & 2022A1515011706 & 2023A1515030157 & 2023A1515011014).

Author Contributions

All authors made a significant contribution to the work reported, whether that is in the conception, study design, analysis and interpretation, or in all these areas; took part in drafting, revising or critically reviewing the article; gave final approval of the version to be published; have agreed on the journal to which the article has been submitted; and agree to be accountable for all aspects of the work.

Disclosure

Dr Ziwei Huang and Dr Ziren Su report a patent A type of protoberberine-based oxidized cyclodextrin complex and its preparation method and application issued to CN202310409421.9. The authors declare no other conflicts of interest in this work.

References

1. Zhong Y, Jin J, Liu P, et al. Berberine Attenuates Hyperglycemia by Inhibiting the Hepatic Glucagon Pathway in Diabetic Mice. *Oxid Med Cell Longev*. 2020;2020:6210526. doi:10.1155/2020/6210526
2. Cui HX, Hu YN, Li JW, Yuan K. Hypoglycemic Mechanism of the Berberine Organic Acid Salt under the Synergistic Effect of Intestinal Flora and Oxidative Stress. *Oxid Med Cell*. 2018;2018:8930374. doi:10.1155/2018/8930374
3. Wu C, Zhao Y, Zhang Y, et al. Gut microbiota specifically mediates the anti-hypercholesterolemic effect of berberine (BBR) and facilitates to predict BBR's cholesterol-decreasing efficacy in patients. *J Adv Res*. 2022;37:197–208.
4. Xing L, Zhou X, Li AH, et al. Atheroprotective Effects and Molecular Mechanism of Berberine. *Front Mol Biosci*. 2021;8:762673. doi:10.3389/fmolb.2021.762673
5. Shou JW, Li XX, Tang YS, et al. Novel mechanistic insight on the neuroprotective effect of berberine: the role of PPARδ for antioxidant action. *Free Radic Biol Med*. 2022;181:62–71. doi:10.1016/j.freeradbiomed.2022.01.022
6. Li Q, Huang Z, Liu D, et al. Effect of Berberine on Hyperuricemia and Kidney Injury: a Network Pharmacology Analysis and Experimental Validation in a Mouse Model. *Drug Des Devel Ther*. 2021;15:3241–3254. doi:10.2147/dddt.S317776
7. Li C, Ai G, Wang Y, et al. Oxyberberine, a novel gut microbiota-mediated metabolite of berberine, possesses superior anti-colitis effect: impact on intestinal epithelial barrier, gut microbiota profile and TLR4-MyD88-NF-κB pathway. *Pharmacol Res*. 2020;152:104603. doi:10.1016/j.phrs.2019.104603
8. Chen HB, Luo CD, Ai GX, et al. A comparative investigation of the interaction and pharmacokinetics of hemoglobin with berberine and its oxymetabolite. *J Pharm Biomed*. 2021;199:114032. doi:10.1016/j.jpba.2021.114032
9. Li QP, Dou YX, Huang ZW, et al. Therapeutic effect of oxyberberine on obese non-alcoholic fatty liver disease rats. *Phytomedicine*. 2021;85:153550. doi:10.1016/j.phymed.2021.153550
10. Li CL, Tan LH, Wang YF, et al. Comparison of anti-inflammatory effects of berberine, and its natural oxidative and reduced derivatives from Rhizoma Coptidis *in vitro* and *in vivo*. *Phytomedicine*. 2019;52:272–283. doi:10.1016/j.phymed.2018.09.228
11. Dou Y, Huang R, Li Q, et al. Oxyberberine, an absorbed metabolite of berberine, possess superior hypoglycemic effect via regulating the PI3K/Akt and Nrf2 signaling pathways. *Biomed Pharmacother*. 2021;137:111312. doi:10.1016/j.biopha.2021.111312
12. Dou Y, Ai G, Huang R, et al. *In vitro* and *in vivo* hypoglycemia effect of oxyberberine, a novel HO-1 agonist: a renewed evidence linking HO-1 to diabetes mellitus. *Phytomedicine*. 2022;101:154135. doi:10.1016/j.phymed.2022.154135
13. Singh S, Verma M, Malhotra M, Prakash S, Singh TD. Cytotoxicity of alkaloids isolated from Argemone mexicana on SW480 human colon cancer cell line. *Pharm Biol*. 2016;54(4):740–745. doi:10.3109/13880209.2015.1073334
14. Sun L, He M, Li F, et al. Oxyberberine sensitizes liver cancer cells to sorafenib via inhibiting NOTCH1-USP7-c-Myc pathway. *Hepatol commun*. 2024;8(4):405. doi:10.1097/hc9.0000000000000405
15. Ai G, Wu X, Dou Y, et al. Oxyberberine, a novel HO-1 agonist, effectively ameliorates oxidative stress and inflammatory response in LPS/D-GalN induced acute liver injury mice via coactivating erythrocyte metabolism and Nrf2 signaling pathway. *Food Chem Toxicol*. 2022;166:113215. doi:10.1016/j.fct.2022.113215
16. Zhao S, Li J, Xing X, Chen J, Zhou Q, Sun J. Oxyberberine suppressed the carbon tetrachloride-induced liver fibrosis by inhibiting liver inflammation in a sirtuin 3-dependent manner in mice. *Int Immunopharmacol*. 2023;116:109876. doi:10.1016/j.intimp.2023.109876
17. Xu L. *Hypouricemic Effect of Phellodendri Cortex and Metabolites of Its Main Components in Hyperuricemic Mice*. Guangzhou university of chinese medicine; 2022.
18. Su Z, Chen J, Li Y, et al. Application of oxyberberine in preparation of drugs for metabolic diseases, and pharmaceutical composition comprising oxyberberine. *J Med*. 2022.
19. Yang LJ, Ma SX, Zhou SY, et al. Preparation and characterization of inclusion complexes of naringenin with β-cyclodextrin or its derivative. *Carbohydr Polym*. 2013;98(1):861–869. doi:10.1016/j.carbpol.2013.07.010
20. Alshati F, Alahmed TAA, Sami F, et al. Guest-host Relationship of Cyclodextrin and its Pharmacological Benefits. *Curr Pharm Des*. 2023;29(36):2853–2866. doi:10.2174/0113816128266398231027100119
21. Adamkiewicz L, Szeleszczuk L. Review of Applications of Cyclodextrins as Taste-Masking Excipients for Pharmaceutical Purposes. *Molecules*. 2023;28(19):658.

22. Gamboa-Arancibia ME, Caro N, Gamboa A, et al. Improving Lurasidone Hydrochloride's Solubility and Stability by Higher-Order Complex Formation with Hydroxypropyl-β-cyclodextrin. *Pharmaceutics*. 2023;15(1).
23. Davoudi-Monfared E, Ahmadi A, Karimpour-Razkenari E, Shahrami B, Najmeddin F, Mojtahedzadeh M. Remdesivir Administration in COVID-19 Patients With Renal Impairment: a Systematic Review. *Am J Ther*. 2022;29(5):e520–e533. doi:10.1097/mjt.0000000000001543
24. Zoeller T, Dressman JB, Klein S. Application of a ternary HP-β-CD-complex approach to improve the dissolution performance of a poorly soluble weak acid under biorelevant conditions. *Int J Pharm*. 2012;430(1–2):176–183. doi:10.1016/j.ijpharm.2012.04.029
25. Dahan A, Beig A, Lindley D, Miller JM. The solubility-permeability interplay and oral drug formulation design: two heads are better than one. *Adv Drug Deliv*. 2016;101:99–107. doi:10.1016/j.addr.2016.04.018
26. Taylor LS, Zhang GGZ. Physical chemistry of supersaturated solutions and implications for oral absorption. *Adv Drug Deliv*. 2016;101:122–142. doi:10.1016/j.addr.2016.03.006
27. Maghsoodi M, Nokhodchi A, Oskuei MA, Heidari S. Formulation of Cinnarizine for Stabilization of Its Physiologically Generated Supersaturation. *AAPS Pharm Sci Tech*. 2019;20(3):139. doi:10.1208/s12249-019-1338-7
28. Jo K, Kim H, Khadka P, et al. Enhanced intestinal lymphatic absorption of saquinavir through supersaturated self-microemulsifying drug delivery systems. *Asian J. Pharm. Sci*. 2020;15(3):336–346. doi:10.1016/j.ajps.2018.11.009
29. Raghavan SL, Kiepfer B, Davis AF, Kazarian SG, Hadgraft J. Membrane transport of hydrocortisone acetate from supersaturated solutions; the role of polymers. *Int J Pharm*. 2001;221(1–2):95–105. doi:10.1016/s0378-5173(01)00673-1
30. Raghavan SL, Trividic A, Davis AF, Hadgraft J. Effect of cellulose polymers on supersaturation and *in vitro* membrane transport of hydrocortisone acetate. *Int J Pharm*. 2000;193(2):231–237. doi:10.1016/s0378-5173(99)00345-2
31. Gratieri T, Pinho LAG, Oliveira MA, et al. Hydroxypropyl-β-cyclodextrin-complexed naringenin by solvent change precipitation for improving anti-inflammatory effect *in vivo*. *Carbohydr Polym*. 2020;231:115769. doi:10.1016/j.carbpol.2019.115769
32. Tao C, Huo T, Zhang Q, Song H. Effect of Soluplus on the supersaturation and absorption of tacrolimus formulated as inclusion complex with dimethyl-β-cyclodextrin. *Pharm Dev Technol*. 2019;24(9):1076–1082. doi:10.1080/10837450.2019.1630651
33. Brewster ME, Loftsson T. Cyclodextrins as pharmaceutical solubilizers. *Adv Drug Deliv*. 2007;59(7):645–666. doi:10.1016/j.addr.2007.05.012
34. Brewster ME, Vandecruys R, Peeters J, Neeskens P, Verreck G, Loftsson T. Comparative interaction of 2-hydroxypropyl-beta-cyclodextrin and sulfobutylether-beta-cyclodextrin with itraconazole: phase-solubility behavior and stabilization of supersaturated drug solutions. *Eur J Pharm Sci*. 2008;34(2–3):94–103. doi:10.1016/j.ejps.2008.02.007
35. Liu M, Higashi K, Ueda K, Moribe K. Supersaturation maintenance of carvedilol and chlorthalidone by cyclodextrin derivatives: pronounced crystallization inhibition ability of methylated cyclodextrin. *Int J Pharm*. 2023;637:122876. doi:10.1016/j.ijpharm.2023.122876
36. Soe H, Sripetch S, Loftsson T, Stefánsson E, Jansook P. Effect of Soluplus(®) on γ-cyclodextrin solubilization of irbesartan and candesartan and their nanoaggregates formation. *Pharm Dev Technol*. 2022;27(1):9–18. doi:10.1080/10837450.2021.2017968
37. Ren L, Wang J, Chen G. Preparation, optimization of the inclusion complex of glaucocalyxin A with sulfobutylether-β-cyclodextrin and antitumor study. *Drug Deliv*. 2019;26(1):309–317. doi:10.1080/10717544.2019.1568623
38. Durand A, Mathiron D, Rigaud S, Djedaini-Pilard F, Marçon F. Rapid Study on Mefloquine Hydrochloride Complexation with Hydroxypropyl-β-Cyclodextrin and Randomly Methylated β-Cyclodextrin: phase Diagrams, Nuclear Magnetic Resonance Analysis, and Stability Assessment. *Pharmaceutics*. 2023;15(12).
39. Gurunath S, Nanjwade BK, Patila PA. Enhanced solubility and intestinal absorption of candesartan cilexetil solid dispersions using everted rat intestinal sacs. *Saudi Pharm J*. 2014;22(3):246–257. doi:10.1016/j.jsps.2013.03.006
40. Chen B, Wang X, Zhang Y, et al. Improved solubility, dissolution rate, and oral bioavailability of main biflavonoids from Selaginella doederleinii extract by amorphous solid dispersion. *Drug Deliv*. 2020;27(1):309–322. doi:10.1080/10717544.2020.1716876
41. Li C, Liu M, Deng L, Luo D, Ma R, Lu Q. Oxyberberine ameliorates TNBS-induced colitis in rats through suppressing inflammation and oxidative stress via Keap1/Nrf2/NF-κB signaling pathways. *Phytomedicine*. 2023;116:154899. doi:10.1016/j.phymed.2023.154899
42. Yong T, Li D, Li M, et al. Anti-Hyperuricemic Effect of 2-Hydroxy-4-methoxy-benzophenone-5-sulfonic Acid in Hyperuricemic Mice through XOD. *Molecules*. 2018;23.
43. Yong T, Chen S, Xie Y, et al. Cordycepin, a Characteristic Bioactive Constituent in Cordyceps militaris, Ameliorates Hyperuricemia through URAT1 in Hyperuricemic Mice. *Front Microbiol*. 2018;9:58. doi:10.3389/fmicb.2018.00058
44. Kim CW, Sung JH, Kwon JE, et al. Toxicological Evaluation of Saposhnikoviae Radix Water Extract and its Antihyperuricemic Potential. *Toxicol Res*. 2019;35(4):371–387. doi:10.5487/tr.2019.35.4.371
45. Higuchi T. Phase solubility techniques. *Adv Anal Chem Instrum*. 1965;4:117–212.
46. Suvarna V, Gujar P, Murahari M. Complexation of phytochemicals with cyclodextrin derivatives - An insight. *Biomed Pharmacother*. 2017;88:1122–1144. doi:10.1016/j.biopha.2017.01.157
47. Yin LF, Huang SJ, Zhu CL, et al. *In vitro* and *in vivo* studies on a novel solid dispersion of repaglinide using polyvinylpyrrolidone as the carrier. *Drug Dev Ind Pharm*. 2012;38(11):1371–1380. doi:10.3109/03639045.2011.652635
48. Sun DZ, Li L, Qiu XM, Liu F, Yin BL. Isothermal titration calorimetry and 1H NMR studies on host-guest interaction of paeonol and two of its isomers with beta-cyclodextrin. *Int J Pharm*. 2006;316(1–2):7–13. doi:10.1016/j.ijpharm.2006.02.020
49. Schneider HJ, Hacket F, Rüdiger V, Ikeda H. NMR Studies of Cyclodextrins and Cyclodextrin Complexes. *Chem Rev*. 1998;98(5):1755–1786. doi:10.1021/cr970019t
50. Kamigauchi M, Kanbara N, Sugiura M, Iwasa K, Ohishi H, Ishida T. Berberine/γ-Cyclodextrin Inclusion Structure Studied by 1H-NMR Spectroscopy and Molecular-Dynamics Calculations. *Helvetica Chim Acta*. 2004;87(1):264–271. doi:10.1002/hlca.200490013
51. Adhikari S, Daftardar S, Fratev F, et al. Elucidation of the orientation of selected drugs with 2-hydroxylpropyl-β-cyclodextrin using 2D-NMR spectroscopy and molecular modeling. *Int J Pharm*. 2018;545(1–2):357–365. doi:10.1016/j.ijpharm.2018.05.016
52. Singh D, Singh M, Tharmatt A, Tiwary AK, Bedi N. Polymeric precipitation inhibitor as an effective trigger to convert supersaturated into supersaturable state in vivo. *Ther Deliv*. 2019. doi:10.4155/tde-2019-0053
53. Li YW, Zhang HM, Cui BJ, et al. "Felodipine-indomethacin" co-amorphous supersaturating drug delivery systems: "Spring-parachute" process, stability, *in vivo* bioavailability, and underlying molecular mechanisms. *Eur J Pharm Biopharm*. 2021;166:111–125. doi:10.1016/j.ejpb.2021.05.030
54. Jansook P, Ogawa N, Loftsson T. Cyclodextrins: structure, physicochemical properties and pharmaceutical applications. *Int J Pharm*. 2018;535(1–2):272–284. doi:10.1016/j.ijpharm.2017.11.018

55. Coleman AW, Nicolis I, Keller N, Dalbiez JP. Aggregation of cyclodextrins: an explanation of the abnormal solubility of β-cyclodextrin. *J Incl Phenom Macrocyclic Chem*. 1992;13:139–143.
56. Do TT, Van Hooghten R, Van den Mooter G. A study of the aggregation of cyclodextrins: determination of the critical aggregation concentration, size of aggregates and thermodynamics using isodesmic and K(2)-K models. *Int J Pharm*. 2017;521(1–2):318–326. doi:10.1016/j.ijpharm.2017.02.037
57. Messner M, Kurkov SV, Brewster ME, Jansook P, Loftsson T. Self-assembly of cyclodextrin complexes: aggregation of hydrocortisone/cyclodextrin complexes. *Int J Pharm*. 2011;407(1–2):174–183. doi:10.1016/j.ijpharm.2011.01.011
58. Chen W, Miao YQ, Fan DJ, et al. Bioavailability study of berberine and the enhancing effects of TPGS on intestinal absorption in rats. *AAPS Pharm Sci Tech*. 2011;12(2):705–711. doi:10.1208/s12249-011-9632-z
59. Huang Z, Li M, Qin Z, et al. Intestines-erythrocytes-mediated bio-disposition deciphers the hypolipidemic effect of berberine from Rhizoma Coptidis: a neglected insight. *J Ethnopharmacol*. 2023;314:116600. doi:10.1016/j.jep.2023.116600
60. Fong SY, Bauer-Brandl A, Brandl M. Oral bioavailability enhancement through supersaturation: an update and meta-analysis. *Expert Opinion Drug Deliv*. 2017;14(3):403–426. doi:10.1080/17425247.2016.1218465